Research in Astronomy and Astrophysics, 25:025006 (14pp), 2025 February

https://doi.org/10.1088/1674-4527/ada424
CSTR: 32081.14.RAA.ada424

O'Connell Effect and Period Variations on Solar-like Contact Binary EF Boo

Jing-Jing Wang[1], Meng Guo[2], Xiao-Man Tian[3], and Bin Zhang[4]
[1] China University of Petroleum–Beijing at Karamay, Karamay 834000, China; wangjingjing@cupk.edu.cn
[2] China University of Petroleum–Beijing, Beijing 102249, China
[3] School of Aeronautics, Shandong Jiaotong University, Jinan 250000, China
[4] School of Physics and Electronic Science, Guizhou Normal University, Guiyang 550025, China
Received 2024 October 8; revised 2024 December 13; accepted 2024 December 30; published 2025 January 27

Abstract

Using ground-based telescopes, the multi-color photometric observations of the contact binary EF Boo were obtained in 2020, 2023, and 2024. Combining these with 7-sectors of light curves from TESS data, the variations of the O'Connell effect in continuous time and shapes of light curves over several years were identified. Three sets of typical light curves were analyzed to determine the photometric solutions via the Wilson–Devinney program. Considering the spectroscopic mass ratio of $q = 0.53$, these photometric solutions suggest that EF Boo is a W-type W UMa contact binary with the averaged filling factor of $f = 22.26\%$, a small temperature difference, and a cool spot on the primary component. If the variations of the O'Connell effect are due to the magnetic activity of this cool spot, the longitudinal location varied from $50^{\circ}.4$ to $302^{\circ}.7$ over the time interval of 1434 days. Based on all CCD minimum times from ground-based telescope and TESS data, the $O - C$ curve was also analyzed. A cyclic oscillation ($A_3 = 0.00575$ days, $T_3 = 27.8$ yr) superimposed on a secular increase ($dP/dt = 6.74 \times 10^{-8}$ day yr^{-1}) was discovered for the first time. The successive increase is possibly a result of mass transfer from the less massive star to the more massive one. The cyclic oscillations were possibly explained by the light-travel time effect via a third body or the magnetic activities. From the short cadence observations from TESS, we also calculated the value of the O'Connell effect and $O - C$ value for each cycle and found no correlation between the O'Connell effect and $O - C$ over nearly 30 days across different sectors.

Key words: (stars:) binaries (including multiple): close – (stars:) binaries: eclipsing – stars: solar-type – stars: individual (EF Boo)

1. Introduction

During the orbital period of contact binaries, two distinct eclipses and two intervening maxima are observed. As a result of the physical structure and tidal locking effects, the maximum brightness or flux should be the same theoretically. However, variations in the brightness maxima of these photometric light curves (LC) have been noted by Roberts (1906), Mergentaler (1950), O'Connell (1951), and known as the O'Connell effect, what was first investigated on contact binary RT Lac by Milone (1968). A search on the O'Connell effect in 5374 eclipsing binary stars from the ASAS database (Papageorgiou et al. 2014), pointed out that the range of magnitude difference between the two maxima, |MaxI–MaxII| is 0.025–0.1 mag. Knote et al. (2022) analyzed Kepler eclipsing binaries and characterized a set of 212 systems with a maximum flux difference of at least 1%, suggesting that interaction between closely orbiting components leads to the O'Connell effect ultimately. Among 107 contact binaries from the Hipparcos satellite, these phenomena in late-type contact binaries are more common compared with other types, especially noting that the magnitude difference of G-type ones is less than 0.04 mag (Pribulla et al. 2011; Hwang & Zakamska 2020), such as EQ Tau, FG Hya, UV Lyn, KIC 7284688.

The O'Connell effect and its variations in late-type binaries are often attributed to magnetic activities of star spots (Mullan 1975; Wilsey & Beaky 2009; Heinze 2023; Liu & Yang 2003). For low-mass, cool-temperature late-type stars, these small amplitude differences in maximum brightness are considered direct evidence of spot activity on the surface of at least one component. Recently, Kouzuma (2019) investigated 102 contact binaries with cool spots and concluded that the magnetic activity in the W-type contact binaries is likely caused by stellar dynamos. Spot locations on five low-mass eclipsing binaries changed over several years, notably, for NSVS 02502726, a starspot longitude region ranging from 180° to 360° indicated a magnetic activity cycle of 5.9 yr (Zhang et al. 2014). Shi et al. (2021) observed that the O'Connell effect, due to spot properties, varies with a cycle length of approximately 2000 days from Kepler and TESS light curves for the Algol-type binary system KIC 06852488.

Table 1
Some Investigations on the Contact Binary EF Boo

Years	O'Connell	Parameters	References
1999	Yes	$M_2/M_1 = 0.57$, $\Delta T = 100$ K, $f = 25\%$	Samec et al. (1999)
2000	Yes		Gothard et al. (2000)
2001	None	W-Type, F5+lateG, period = 0.4205 days	Rucinski et al. (2001)
2004	No	$M_2/M_1 = 0.51$, $\Delta T = 112$ K, $f = 28\%$	Ozdemir et al. (2004)
2004	None	$M_2/M_1 = 0.45$, $f = 20\%$	Selam (2004)
2005	No	$M_2/M_1 = 0.53$, $\Delta T = 25$ K, $f = 18\%$	Gazeas et al. (2005)
2017	None	continuous period increase	Yu et al. (2017)

Table 2
Information for Observations of the Contact Binary EF Boo

Years	Date	Exposure times	Effective field	Camera	Telescope
2020	Mar 16, Apr 28, Jun 13	B 40 s, V 30 s, R_c 20 s, I_c 10s	$13\farcm5 \times 13\farcm5$	2048 × 2048 DZ936N	60 cm
2023	Jun 1, Jun 30	B 10 s, V 5 s,R_cI_c 3s	$16\farcm5 \times 16\farcm5$	1024 × 1024 PI1024 BFT	85 cm
2024	May 20, Jun 14, Jun 16	B 5 s, VR_cI_c 3 s	$16\farcm5 \times 16\farcm5$	1024 × 1024 PI1024 BFT	85 cm

Additionally, the orbital period variations exhibit various behaviors, including successive increases, decreases, and periodic oscillations. Generally, these oscillations are due to a third body around the binary system, though Applegate (1992) suggested that non-strict variations may result from magnetic activities. Yilmaz et al. (2023) studied star spots in contact binary PP Lac, indicating that eclipse timing variation variations (ETVs) are attributed to the magnetic activity cycle combined with the presence of a third body. Using 27 sets of new photometric observations from the last 5 yr, Pi et al. (2019) found that the cyclic oscillation of the O'Connell effect with 5.15 yr is shorter than the 14.58 yr oscillation observed in $O - C$ (observed minus calculated) curve of the orbital period.

We hope to discover solar-like contact binaries with continuous variation on the O'Connell effect, period variations, and spots to further understand the evolution and magnetic activities of binary stars. EF Boo is a W-subtype contact binary discovered by Hoeg et al. (1997). Basic parameters, including G5 and EB-type light curves, were obtained by Perryman et al. (1997). From 1999 to 2017, seven studies presented results summarized in Table 1. This target exhibits the obvious O'Connell effect and variations in light curves, with varying solutions over time. In this work, we monitor EF Boo in 2020, 2023 and 2024 using ground-based telescopes, and obtain TESS observations. These light curves were used for analyzing continuous variations on the O'Connell effect, the orbital period variations, and re-evaluating the photometric solutions. Based on these properties, the O'Connell effect, ternary nature, magnetic activity, and evolution are discussed.

Table 3
Coordinates of the Contact Binary EF Boo (V), the Comparison (C) and the Check Stars (Ch)

Stars	α_{2000}	δ_{2000}	$V_{\rm mag}$
EF Boo(V)	$14^{\rm h}32^{\rm m}30\fs57$	$+50°49'40\farcs69$	9.45
HD 127807(C)	$14^{\rm h}31^{\rm m}46\fs31$	$+50°55'42\farcs46$	8.46
HD 234152(Ch)	$14^{\rm h}33^{\rm m}32\fs05$	$+50°45'11\farcs57$	10.9

2. Observations

2.1. Ground-based Telescope

The multi-color photometric observations listed in Table 2 were carried out with 60 cm, and 85 cm telescopes (Zhou et al. 2009), in different years at XingLong Station of the National Astronomical Observatories of the Chinese Academy of Sciences. On 2020 March 16, due to a malfunction in the filter system, we only obtained the V-band light curve.

All observed images were reduced by the use of the C-MuniPack program (http://c-munipack.sourceforge.net/), including bias correction, flat-fielding, aperture photometry, and differential photometry operations. The variable star (V), the comparison star (C), and the check star (CH) are listed in Table 3. The observational errors in the BVR_cI_c band are less than 0.004 mag. These observations, including their magnitudes and Barycentric Julian Dates (BJD), are depicted in Figure 1. Due to constraints imposed by the weather conditions and the eclipsing period, the complete curves were not obtained

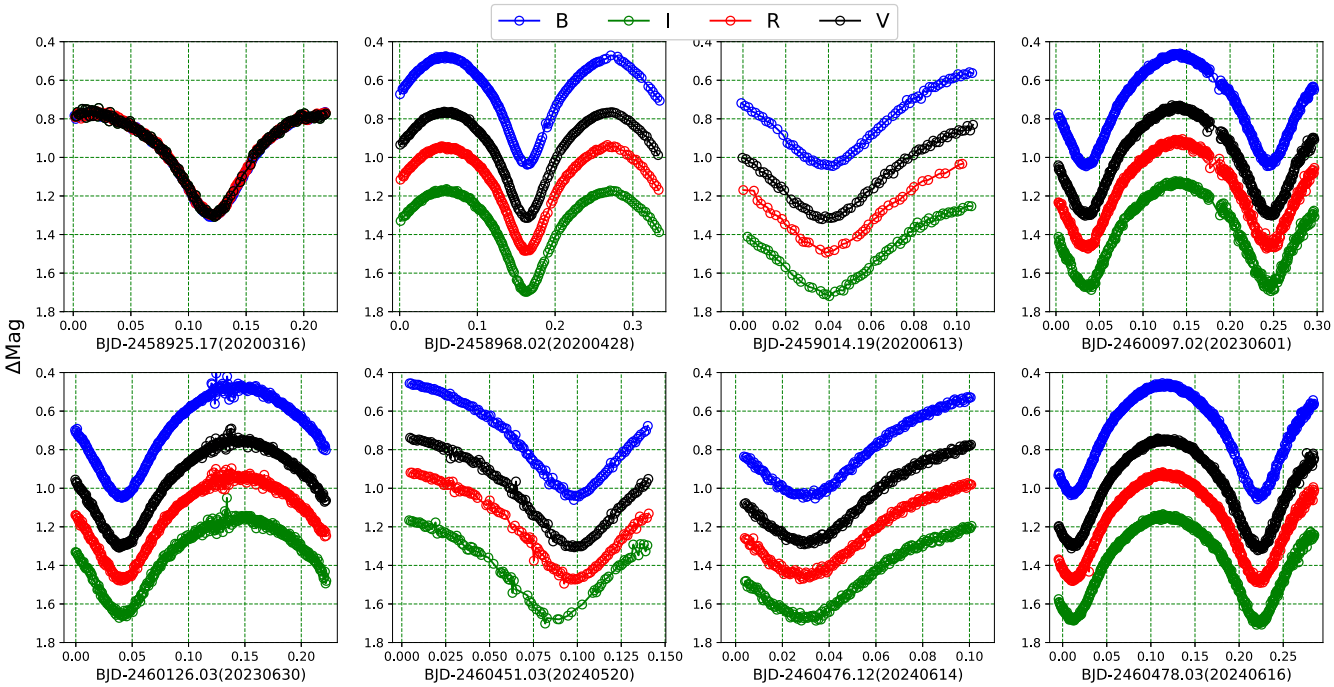

Figure 1. The multi-color BVR_cI_c-band observations in 2020, 2023, and 2024 at XingLong Station.

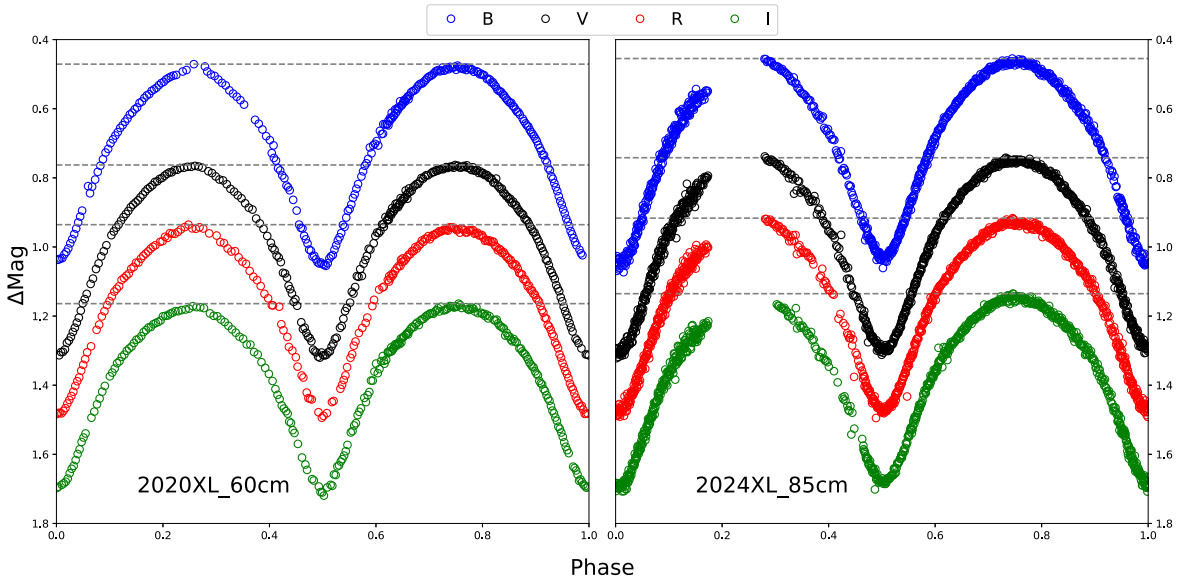

Figure 2. The BVR_cI_c-band light curves in 2020 and 2024 at XingLong Station.

for the entire night. However, the EW-type light curves are clearly discernible.

With the linear ephemeris equation (Yu et al. 2017),

$$\begin{aligned}\text{Min.I(BJD)} = {} & 2452500.2262(2) \\ & + 0\overset{d}{.}42051484(6) \times E, \end{aligned} \quad (1)$$

the light curves (LCs) along with the orbital phase are acquired from three sets of observations in 2020 and 2024. On the left side of Figure 2, these LCs were collected with the 60 cm telescope in 2020, while the right side curves with the 85 cm telescope in 2024. The heights between the maximum light of individual LCs are nearly the same, indicating that there is no O'Connell effect. These curves are helpful to get

Table 4
$O - C$ Values of Light Minimum Times for EF Boo

BJD	Epoch	$(O-C)_1$	$(O-C)_2$	Residuals	Errors	References	BJD	Epoch	$(O-C)_1$	$(O-C)_2$	Residuals	Errors	References
2448500.30247	−9512.0	0.0135	0.0049	0.0001	...	Perryman et al. (1997)	2456747.44167	10100.0	0.0156	0.0060	0.0013	0.003	Hubscher & Lehmann (2015)
2451282.83637	−2895.0	0.0007	−0.0049	−0.0010	0.0006	Samec et al. (1999)	2457144.19867	11043.5	0.0169	0.0065	0.0011	...	Yu et al. (2017)
2451283.67837	−2893.0	0.0017	−0.0039	−0.0001	0.0001	Samec et al. (1999)	2457150.50707	11058.5	0.0176	0.0071	0.0017	0.0019	Hubscher (2016)
2451283.88967	−2892.5	0.0027	−0.0029	0.0010	0.0011	Samec et al. (1999)	2457151.34827	11060.5	0.0177	0.0073	0.0019	0.0011	Hubscher (2016)
2451284.72977	−2890.5	0.0018	−0.0038	0.0000	0.0001	Samec et al. (1999)	2457153.45027	11065.5	0.0172	0.0067	0.0013	0.0022	Hubscher (2016)
2451284.93937	−2890.0	0.0011	−0.0045	−0.0006	0.0006	Samec et al. (1999)	2457464.42048	11805.0	0.0167	0.0055	−0.0002	0.0019	Hubscher (2017)
2451313.11077	−2823.0	−0.0020	−0.0075	−0.0036	...	Guilbault et al. (2001)	2457464.63138	11805.5	0.0173	0.0062	0.0005	0.0016	Hubscher (2017)
2451589.81577	−2165.0	0.0043	−0.0012	0.0034	...	Diethelm (2010)	2457565.34535	12045.0	0.0180	0.0066	0.0009	0.00006	Bahar et al. (2017)
2451677.48956	−1956.5	0.0007	−0.0047	0.0000	...	Safar & Zejda (2002)	2457829.42869	12673.0	0.0180	0.0060	0.0003	0.0009	Pagel (2018)
2451712.39176	−1873.5	0.0002	−0.0052	−0.0004	0.017	Ozdemir et al. (2001)	2457829.63919	12673.5	0.0182	0.0062	0.0005	0.0011	Pagel (2018)
2451719.33076	−1857.0	0.0007	−0.0047	0.0001	0.004	Ozdemir et al. (2001)	2458311.33964	13819.0	0.0189	0.0057	0.0003	0.00003	Ozavci et al. (2019)
2452320.66495	−427.0	−0.0014	−0.0067	−0.0011	0.0003	Drozdz & Ogloza (2005)	2458253.30777	13681.0	0.0181	0.0050	−0.0004	0.00003	Ozavci et al. (2019)
2452382.48205	−280.0	0.0001	−0.0053	0.0004	0.0004	Drozdz & Ogloza (2005)	2458271.38954	13724.0	0.0177	0.0046	−0.0008	0.00003	Ozavci et al. (2019)
2452440.51645	−142.0	0.0034	−0.0019	0.0038	0.0014	Zejda (2004)	2459340.12959	16265.5	0.0193	0.0032	0.0001	0.00002	Park et al. (2024)
2452711.11444	501.5	0.0001	−0.0053	0.0005	...	Yu et al. (2017)	2459661.19335	17029.0	0.0200	0.0028	0.0008	0.00021	Park et al. (2024)
2452711.32524	502.0	0.0006	−0.0047	0.0010	...	Yu et al. (2017)	2459689.15707	17095.5	0.0195	0.0022	0.0002	0.00003	Park et al. (2024)
2452777.34574	659.0	0.0003	−0.0051	0.0007	0.0004	Bakis et al. (2003)	2459753.07560	17247.5	0.0198	0.0023	0.0005	0.00003	Park et al. (2024)
2453029.65443	1259.0	0.0001	−0.0053	0.0002	0.0018	Zejda (2004)	2460035.24043	17918.5	0.0191	0.0007	−0.0001	0.00002	Park et al. (2024)
2453056.56713	1323.0	−0.0001	−0.0056	−0.0000	0.0013	Zejda (2004)	2460367.23744	18708.0	0.0197	0.0001	0.0005	0.00003	Park et al. (2024)
2453105.34728	1439.0	0.0003	−0.0052	0.0003	0.0014	Brt et al. (2007)	2458925.29147	15279.0	0.0191	0.0042	−0.0000	0.00132	our
2453117.12023	1467.0	−0.0012	−0.0067	−0.0012	...	Yu et al. (2017)	2458968.18443	15381.0	0.0195	0.0045	0.0004	0.00016	our
2453120.06383	1474.0	−0.0012	−0.0067	−0.0012	...	Yu et al. (2017)	2459014.22977	15490.5	0.0185	0.0033	−0.0007	0.00044	our
2453120.27413	1474.5	−0.0011	−0.0066	−0.0011	...	Yu et al. (2017)	2460097.05611	18065.5	0.0191	0.0005	−0.0001	0.00011	our
2453163.16843	1576.5	0.0006	−0.0048	0.0006	0.0002	Krajci (2005)	2460097.26607	18066.0	0.0188	0.0002	−0.0004	0.00399	our

Table 4
(Continued)

BJD	Epoch	$(O-C)_1$	$(O-C)_2$	Residuals	Errors	References	BJD	Epoch	$(O-C)_1$	$(O-C)_2$	Residuals	Errors	References
2453208.37322	1684.0	0.0001	−0.0054	−0.0000	0.0014	Brt et al. (2007)	2460126.07164	18134.5	0.0191	0.0004	−0.0000	0.00015	our
2453428.30293	2207.0	0.0005	−0.0051	0.0000	...	Yu et al. (2017)	2460451.12904	18907.5	0.0186	−0.0013	−0.0006	0.00026	our
2453463.62553	2291.0	−0.0001	−0.0057	−0.0007	0.0008	Hubscher et al. (2005)	2460476.15033	18967.0	0.0192	−0.0007	0.0001	0.00120	our
2453476.66263	2322.0	0.0010	−0.0046	0.0004	0.0005	Dvorak (2006)	2460478.04204	18971.5	0.0186	−0.0013	−0.0006	0.00005	our
2453484.65233	2341.0	0.0009	−0.0047	0.0003	0.0003	Dvorak (2006)	2460478.25332	18972.0	0.0196	−0.0003	0.0005	0.00227	our
2453718.03903	2896.0	0.0019	−0.0038	0.0007	0.0001	Nelson (2006)	2457798.52119	12599.5	0.0183	0.0064	0.0007	...	$O-C$ gateway
2453789.31414	3065.5	−0.0002	−0.0060	−0.0017	0.0002	Dogru et al. (2006)	2458216.51260	13593.5	0.0180	0.0050	−0.0005	...	$O-C$ gateway
2453911.47584	3356.0	0.0019	−0.0040	0.0001	0.0013	Hubscher et al. (2006)	2458227.44680	13619.5	0.0188	0.0058	0.0003	...	$O-C$ gateway
2454596.49746	4985.0	0.0048	−0.0016	0.0004	0.0005	Hubscher et al. (2009)	2458490.68980	14245.5	0.0195	0.0058	0.0007	...	$O-C$ gateway
2454958.77177	5846.5	0.0056	−0.0012	−0.0005	0.002	Diethelm (2009)	2458540.51830	14364.0	0.0170	0.0032	−0.0019	...	$O-C$ gateway
2454970.33287	5874.0	0.0026	−0.0043	−0.0036	0.0002	Samolyk (2010)	2458928.44521	15286.5	0.0190	0.0040	−0.0002	...	$O-C$ gateway
2455243.87998	6524.5	0.0048	−0.0024	−0.0027	0.0008	Diethelm (2010)	2458928.65531	15287.0	0.0188	0.0039	−0.0003	...	$O-C$ gateway
2455602.58258	7377.5	0.0082	0.0005	−0.0010	0.0001	Hoňková et al. (2013)	2459025.37531	15517.0	0.0204	0.0052	0.0012	...	$O-C$ gateway
2455643.58379	7475.0	0.0092	0.0015	−0.0002	0.0001	Hoňková et al. (2013)	2459038.40901	15548.0	0.0181	0.0029	−0.0010	...	$O-C$ gateway
2455693.41451	7593.5	0.0089	0.0011	−0.0007	0.0001	Hoňková et al. (2013)	2459062.38262	15605.0	0.0224	0.0071	0.0032	...	$O-C$ gateway
2455694.88578	7597.0	0.0084	0.0006	−0.0012	0.0004	Diethelm (2010)	2459288.19472	16142.0	0.0180	0.0020	−0.0012	...	$O-C$ gateway
2455989.66961	8298.0	0.0113	0.0030	0.0003	0.0001	Hoňková et al. (2013)	2459288.19512	16142.0	0.0184	0.0024	−0.0008	...	$O-C$ gateway
2456013.42808	8354.5	0.0107	0.0024	−0.0005	0.0027	Hubscher et al. (2013)	2459288.19562	16142.0	0.0189	0.0029	−0.0003	...	$O-C$ gateway
2456013.63928	8355.0	0.0116	0.0033	0.0005	0.0003	Hubscher et al. (2013)	2459290.29712	16147.0	0.0179	0.0019	−0.0014	...	$O-C$ gateway
2456013.85188	8355.5	0.0140	0.0057	0.0028	0.0006	Diethelm (2012)	2459290.29782	16147.0	0.0186	0.0026	−0.0007	...	$O-C$ gateway
2456020.15478	8370.5	0.0092	0.0008	−0.0020	...	Yu et al. (2017)	2459290.29882	16147.0	0.0196	0.0036	0.0003	...	$O-C$ gateway
2456036.34758	8409.0	0.0121	0.0038	0.0009	0.0006	Banfi et al. (2012)	2459290.30182	16147.0	0.0226	0.0066	0.0033	...	$O-C$ gateway
2456398.41289	9270.0	0.0142	0.0052	0.0013	0.0001	Diethelm (2010)	2459291.13932	16149.0	0.0190	0.0030	−0.0002	...	$O-C$ gateway
2456728.51907	10055.0	0.0162	0.0066	0.0019	0.0014		2459291.13972	16149.0	0.0194	0.0034	0.0002	...	$O-C$ gateway

Table 4
(Continued)

BJD	Epoch	$(O-C)_1$	$(O-C)_2$	Residuals	Errors	References	BJD	Epoch	$(O-C)_1$	$(O-C)_2$	Residuals	Errors	References
						Hubscher & Lehmann (2015)							
2456730.41067	10059.5	0.0155	0.0059	0.0012	0.0017	Hubscher & Lehmann (2015)	2459291.13982	16149.0	0.0195	0.0035	0.0003	...	$O-C$ gateway
2456730.62127	10060.0	0.0158	0.0062	0.0015	0.0014	Hubscher & Lehmann (2015)	2459296.60582	16162.0	0.0188	0.0028	−0.0004	...	$O-C$ gateway
2456736.50797	10074.0	0.0153	0.0057	0.0010	0.0019	Hubscher & Lehmann (2015)	2459305.43712	16183.0	0.0193	0.0033	0.0001	...	$O-C$ gateway
2456745.33908	10095.0	0.0156	0.0060	0.0013	0.0001	Honkova et al. (2015)	2459305.64662	16183.5	0.0186	0.0025	−0.0007	...	$O-C$ gateway
2456745.54844	10095.5	0.0147	0.0051	0.0004	0.0001	Honkova et al. (2015)	...	...	...	...	...	...	...

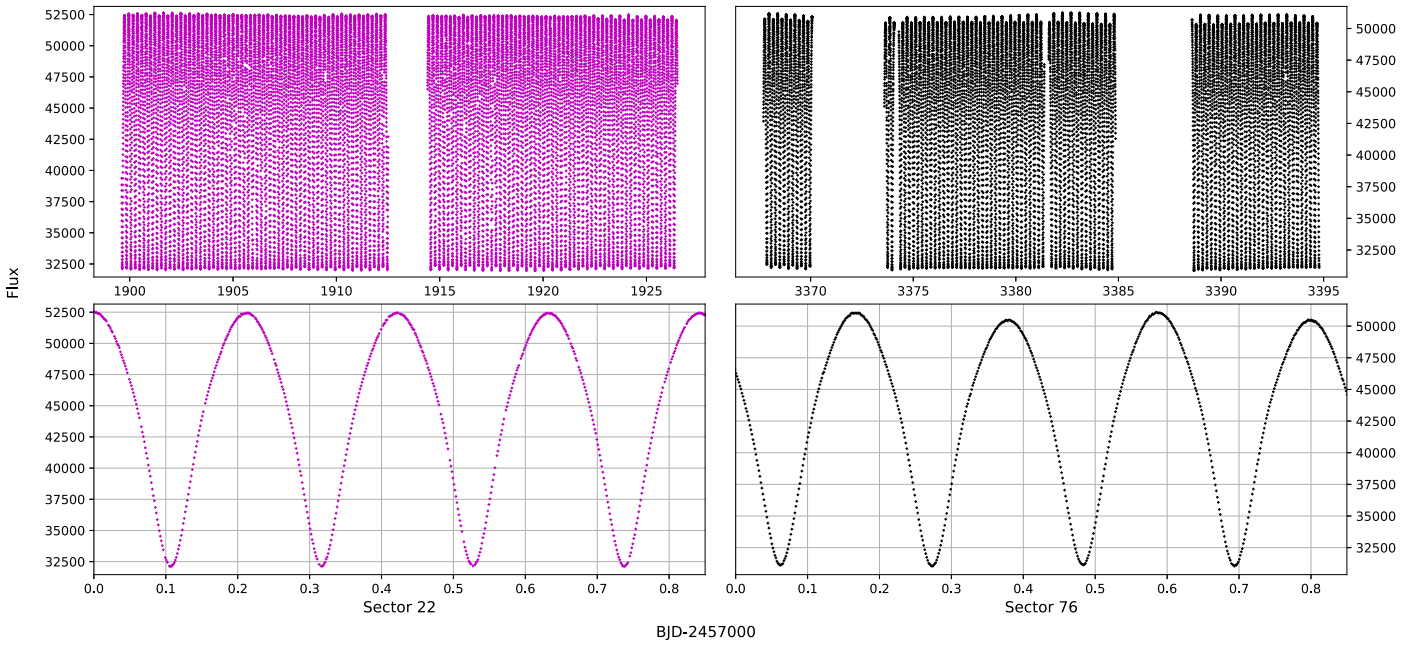

Figure 3. Light curves in Sector 22, 76 for EF Boo from TESS data.

reliable photometric solutions, and several CCD times of minimum light were determined in Table 4. Maybe any small amplitude variations were neglected, we focus on the heights of maximum light (dashed line) in 2020 are obviously different from the ones in 2024, indicating the components are possibly active.

2.2. TESS Light Curves

Transiting Exoplanet Survey Satellite (TESS) provides high-precision continuous light curves with a 2 minute short cadence, available from the MAST website (https://mast.stsci.edu/portal/Mashup/Clients/Mast/Portal.html). From 2019 September to 2024 April, seven sectors' light curves were released, with flux errors of less than 35 e^{-}/s (~0.0008 mag). These observations can be used to analyze small intrinsic variations of the O'Connell effect, as shown in Figure 3. In sector 22, the flux of the primary maximum is equal to the secondary one, but they show a noticeable difference in sector 76. The continuous variations on the O'Connell effect were caught for the first time.

To investigate the intrinsic light variability throughout each complete period, we computed the flux differences around two maxima and minima. Specifically, the fluxes at phases 0.0, 0.25, 0.5, and 0.75 are labeled as Min.I, Max.I, Min.II, and Max.II, respectively. In Figure 4, these fluxes are plotted over time in each sector. The red dots denote Min.I and Max.I, while the black dots represent Min.II and Max.II.

For each period, we also calculated the differences between the maxima and minima. On the left side of Figure 4, the red lines indicate that the flux at Max.I exceeds Max.II (Positive O'Connell effect), while the green lines signify the opposite (Negative O'Connell effect). Similarly, on the right side, these lines represent the minima.

In the last sector in Figure 4 plotted from sector 77 of TESS data, no O'Connell effect is found as the LCs (Ozdemir et al. 2004; Gazeas et al. 2005). Despite the potential influence of systematic telescope errors on these few data points, they hold significant value for other sector light curves. In essence, these differences between two maxima or minima are meaningful.

In the 1st (sector 16), 4th (sector 49), 5th (sector 50), and 6th (sector 76) rows of Figure 4, we see that the flux at the primary maximum and minimum is less than that at the secondary ones. The 2nd (sector 22) and 3rd (sector 23) rows exhibit significant variations, particularly in sector 22, where the effect transitions from negative to positive, with Max.I being brighter than Max.II. These phenomena may result from magnetic activities on the components, such as star spots not only migrating across the stellar surface but also evolving rapidly. These dynamic changes suggest complex underlying processes driving the movement and transformation of these regions, potentially offering deeper insights into stellar magnetic activity and behavior.

3. Variations of Orbital Period

Using light curves from ground-based telescopes and TESS, we have directly determined numerous eclipsing times and compiled additional CCD timings from various literature sources and O-C gateway (http://var2.astro.cz/ocgate/index.php). However, since visual timings with larger errors show considerable scatter (Yu et al. 2017), we have also opted photoelectric and

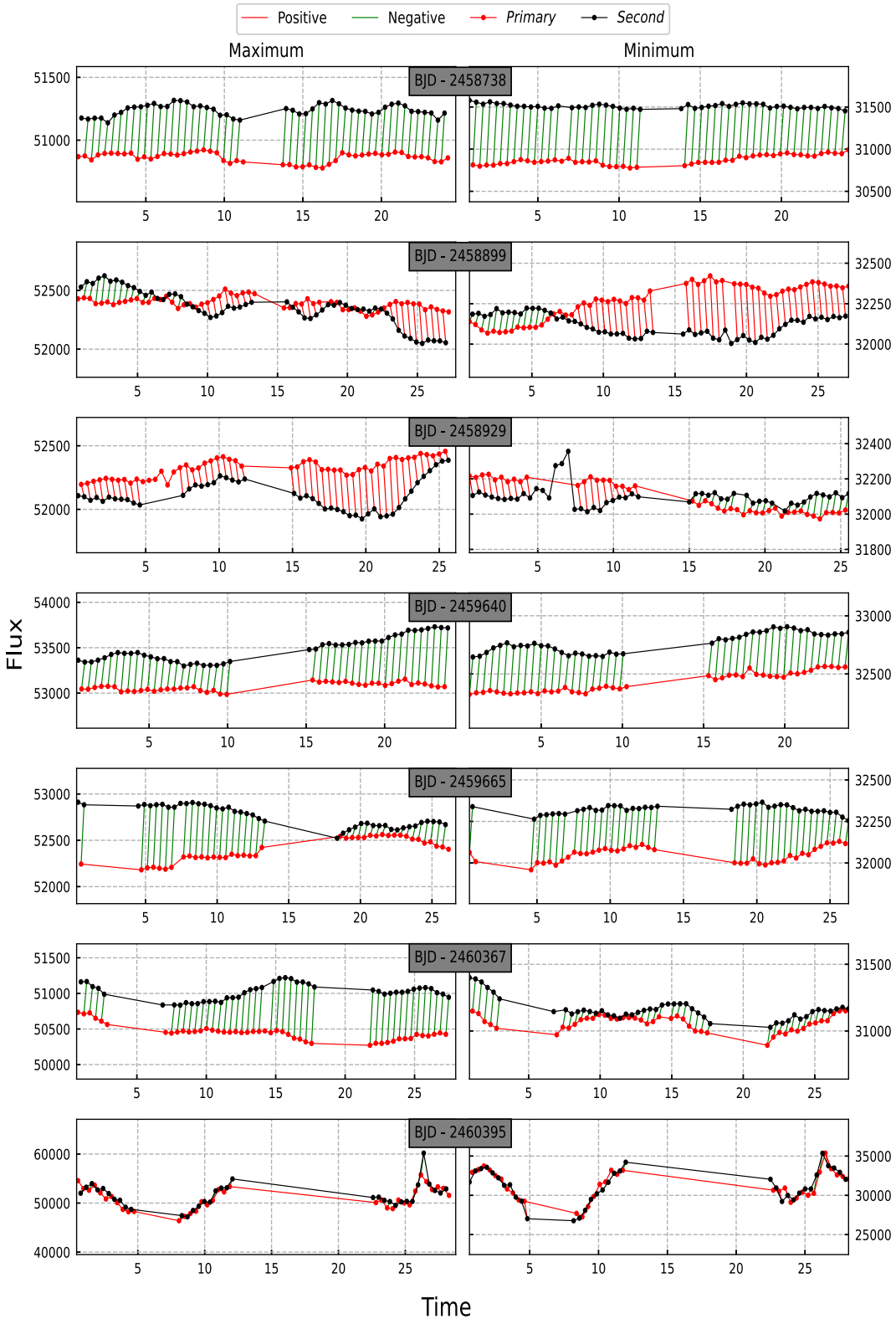

Figure 4. The flux of two maxima and two minima vs. time. Red dots represent the primary maxima, while black dots denote the secondary maxima. Red lines indicate the difference between the primary and secondary maxima, suggesting that the primary maximum or minimum is brighter than the secondary. Conversely, green lines illustrate this difference.

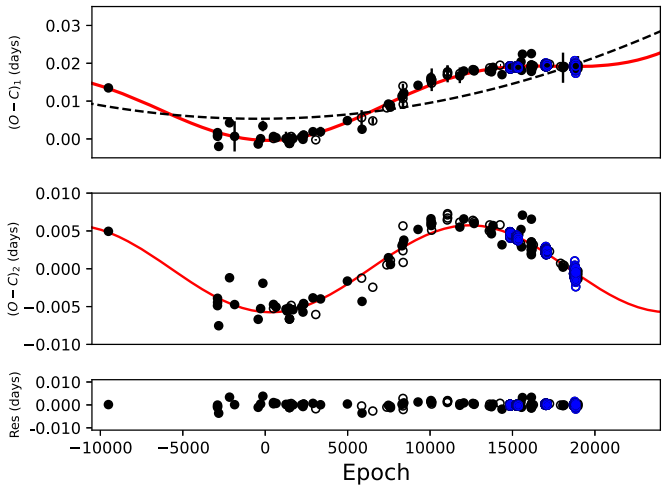

Figure 5. $O-C$ diagram of all available eclipsing times for EF Boo.

CCD data to analyze variations in the orbital period. The Heliocentric Julian Dates (HJD) were converted into barycentric Julian dates (BJD; Eastman et al. 2010). A comprehensive list of all 105 ground-based telescope timings is listed in Table 4, the long-term variation should be analyzed. It is noted that due to the brief duration of the TESS $O-C$ values, 346 data points in our analysis are not provided individually.

Based on the ephemeris Equation (1), we calculated the $(O-C)_1$ values listed in Table 4, which were plotted in the upper panel of Figure 5. The solid circle represent the primary minimum times, the hollow circle for the secondary ones, and the blue refer to the time derived from TESS data. Considering the continuous period increase reported by Yu et al. (2017), we also applied a parabolic fit to the $(O-C)_1$, indicated by the dashed lines. Additionally, after subtracting the long-term increase, a cyclic term was identified and shown in the middle panel. The final residuals are listed in Table 4 and plotted at the bottom of Figure 5, supporting the reliability of the combination of the cyclic and parabolic ephemeris.

The fitting results yield the following equation using the methods from Irwin (1952), Sterken (2005),

$$\mathrm{T} = T_0 + P_0 E + \frac{1}{2}\frac{dP}{dt} P E^2 + A_3 \sin(\omega E + \phi) \qquad (2)$$

where A_3 is the amplitude of sinusoidal variation, T_3 is the period of the cycle, $\omega(=\frac{360^\circ}{T_3}P)$ is the angle per unit epoch, and ϕ is the phase. The new ephemeris is derived as,

$$\begin{aligned}\mathrm{Min.I(BJD)} = {} & 2452500.23148(\pm 0.00009) \\ & + 0^d.42051487(\pm 0.00000003) \times E \\ & + 3.88(\pm 0.02) \times 10^{-11} \times E^2 \\ & + 0.00575(\pm 0.00009)\sin[0^\circ.014914 \times E \\ & + 85^\circ.05(\pm 1^\circ.22)].\end{aligned} \qquad (3)$$

The second-order term suggests a long-term period increase at a rate of $dP/dt = 6.74 \times 10^{-8}$ day yr^{-1}, the sinusoidal oscillation indicates an amplitude of 0.00575 days and a period of 27.8 yr.

The cyclic oscillations in the $O-C$ diagram were commonly attributed to the light-travel time effect caused by the presence of a third body. However, Applegate (1992) suggested that these oscillations may result from magnetic activities. The hypothesis is that the O'Connell effect is a significant indicator of magnetic spot activity. Due to the discontinuous nature of ground-based observations taken at different times, we cannot capture the continuous variation of the O'Connell effect, and explore its relationship with $O-C$ changes thoroughly. Koju & Beaky (2015) found no correlation between the O'Connell effect and orbital period change for SW Lac, CN And and V502 Oph. The period of the O'Connell effect was found shorter than the cyclic oscillations in the $O-C$ diagram for eclipsing binary DV Psc (Pi et al. 2019). From the short cadence observations from TESS, we simply calculated the value of the O'Connell effect and $O-C$ for each cycle. In Figure 6, on the left, the flux difference between two maxima is plotted as black dots, showing noticeable variations of the O'Connell effect without apparent regularity. On the right, the $O-C$ of Min.I times were represented as red dots, and Min.II times as black dots. We also found no correlation between the O'Connell effect and $O-C$ over nearly 30 days across different sectors.

4. Photometric Solutions by the W-D Code

From Table 1, it is evident that the parameters derived from these investigations are different, such as the mass ratio, the temperature difference and the degree of fill-out. However, Gazeas et al. (2005) determined the spectroscopic mass ratio of $M_2/M_1 = 0.53$, where M_1 represents the primary star (the star eclipsed at the primary light minimum).

In our study, photometric solutions were obtained using the W-D program (Wilson & Devinney 1971; Wilson 1990; Wilson & Van Hamme 2014; Wilson 2020). According to the TESS Input Catalog (v8.0) (Stassun et al. 2019), the new effective temperature of the more massive component was fixed at $T = 6320$ K, corresponding to an F-type star. Considering the convective atmospheres of the components, the same values of the gravity-darkening coefficients and the bolometric albedo, i.e., $g_1 = g_2 = 0.32$ (Lucy 1967) and $A_1 = A_2 = 0.5$ (Ruciński 1969) were taken into the model.

Since the symmetric complete light curves were only available in 2020 using the 60 cm telescope, we used these data to look for the converged solutions. The spectroscopic mass ratio 0.53 was compiled for the W-D code. The

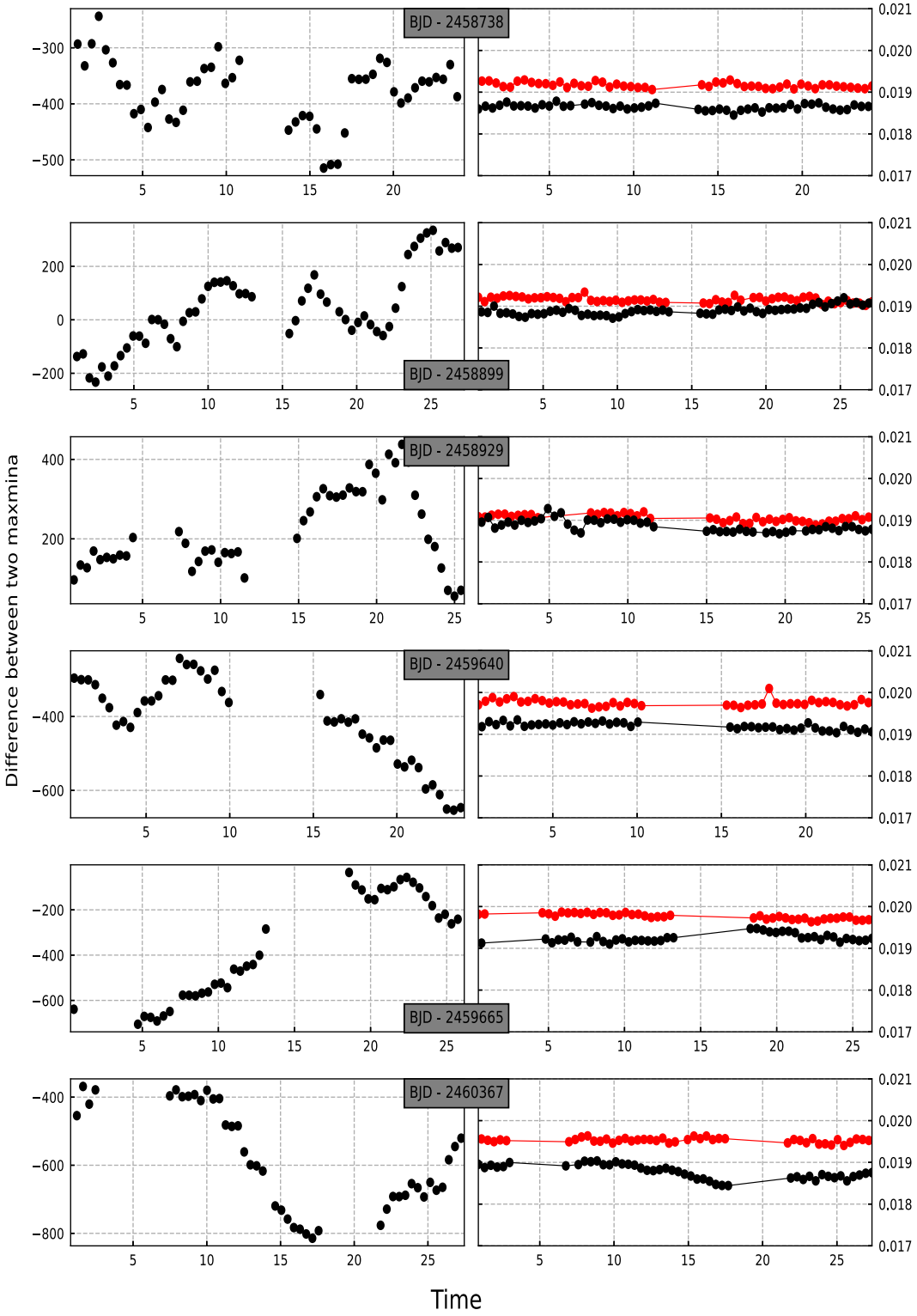

Figure 6. The O'Connell effect and $O - C$ values of 6-sectors continuous TESS data. On the left, the flux difference between two maxima is plotted as black dots. On the right, the $O - C$ of Min.I times were represented as red dots, and Min.II times as black dots.

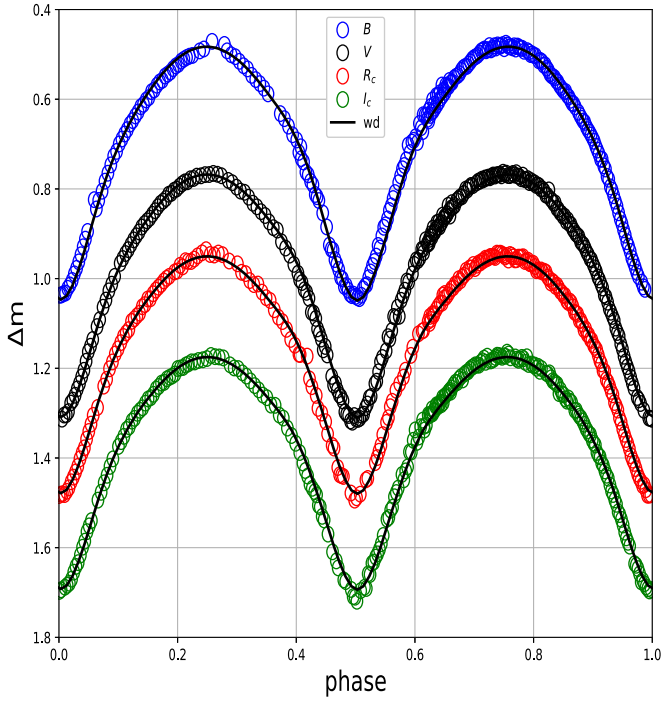

Figure 7. Theoretical light curves observed in 2020.

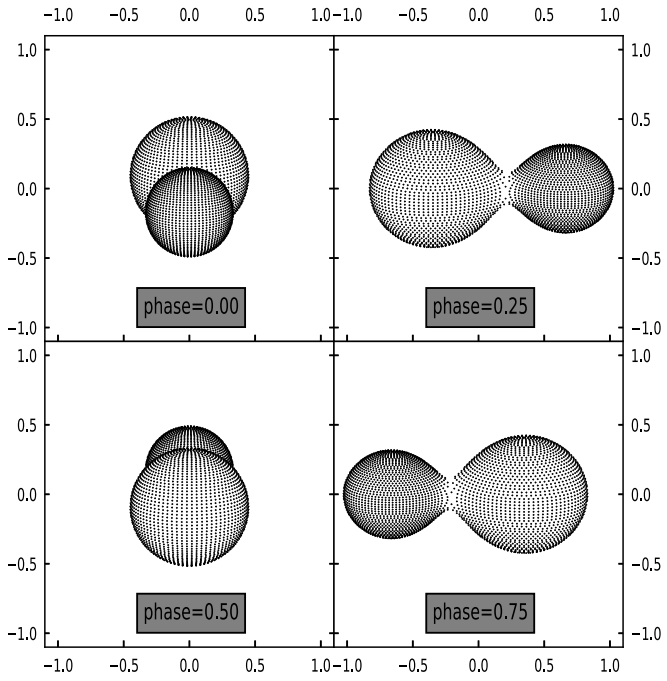

Figure 8. Configurations at phase 0.00, 0.25, 0.50, 0.75.

theoretical light curves are shown in Figure 7, and the configurations at phases are displayed in Figure 8.

Additionally, the light curves of TESS data exhibit the O'Connell effect along with significant variations, indicating magnetic activity on the surface of the component. The maximum flux difference between maxima in positive O'Connell effect light curves is 423 e^{-}/s, while in negative curves, the maximum difference is -825 e^{-}/s. We took them displayed in Figure 9 separately, to derive converted solutions and configurations with dark spots. Remarkably, it is discovered the migration of the cool spot from $50^{\circ}.4$ to $302^{\circ}.7$ on the primary component.

The derived results are detailed in Table 5, notably, the identified errors are exclusively a product of the fitting process within the WD code. These parameters indicate that EF Boo is a W-type shallow-contact binary, the effective temperatures of the two components are nearly identical with an averaged fill-out of 22.26%.

5. Discussion and Conclusion

In 2020, 2023, 2024, we carried out multi-color BVR_cI_c–band observations using ground-based telescopes several times. In these light curves, although the O'Connell effect was absent, significant variations were noted across different years. Additionally, analysis of 7-sectors light curves from the TESS data revealed the presence of a variable O'Connell effect. As presented by Samec et al. (1999), Gothard et al. (2000), these phenomena suggest that contact binary EF Boo may be active.

The complete light curves obtained in 2020, along with two TESS light curves exhibiting O'Connell effects, were used to analyze the photometric solutions of these contact binaries. These solutions suggest that this system is a typical W-type contact binary with a degree of contact of $f = 22.26\%$, a mass ratio of $q = M_2/M_1 = 0.53$, and a small temperature difference between two components, indicating both components share a common convective envelope. These results could confirm the parameters calculated by Selam (2004), and Gazeas et al. (2005).

From the positive O'Connell effect in the light curve, we derived the presence of one cool spot, adjusting its location to fit the negative curve accurately. Thus, it is inferred that this spot is migrating, causing the O'Connell effect and light curve variations. In the light curves of the two O'Connell effects, the flux differences are at the maximum and minimum values, respectively, with a time interval of 1434 days. If this variation in the O'Connell effect is due to this cool spot, the longitudinal location varied from $50^{\circ}.4$ to $302^{\circ}.7$ over the same time interval.

The $O - C$ diagram shown in Figure 5 reveals a long-term increase and the cyclic oscillation. The orbital period of EF Boo is increasing at a rate of $dP/dt = 6.74 \times 10^{-8}$ day yr^{-1}. The absolute parameters of this system were estimated as $M_1 = 1.547\,M_{\odot}$, $R_1 = 1.431\,R_{\odot}$ and $M_2 = 0.792\,M_{\odot}$, $R_2 = 1.0641\,R_{\odot}$ (Gazeas et al. 2005). Using the following

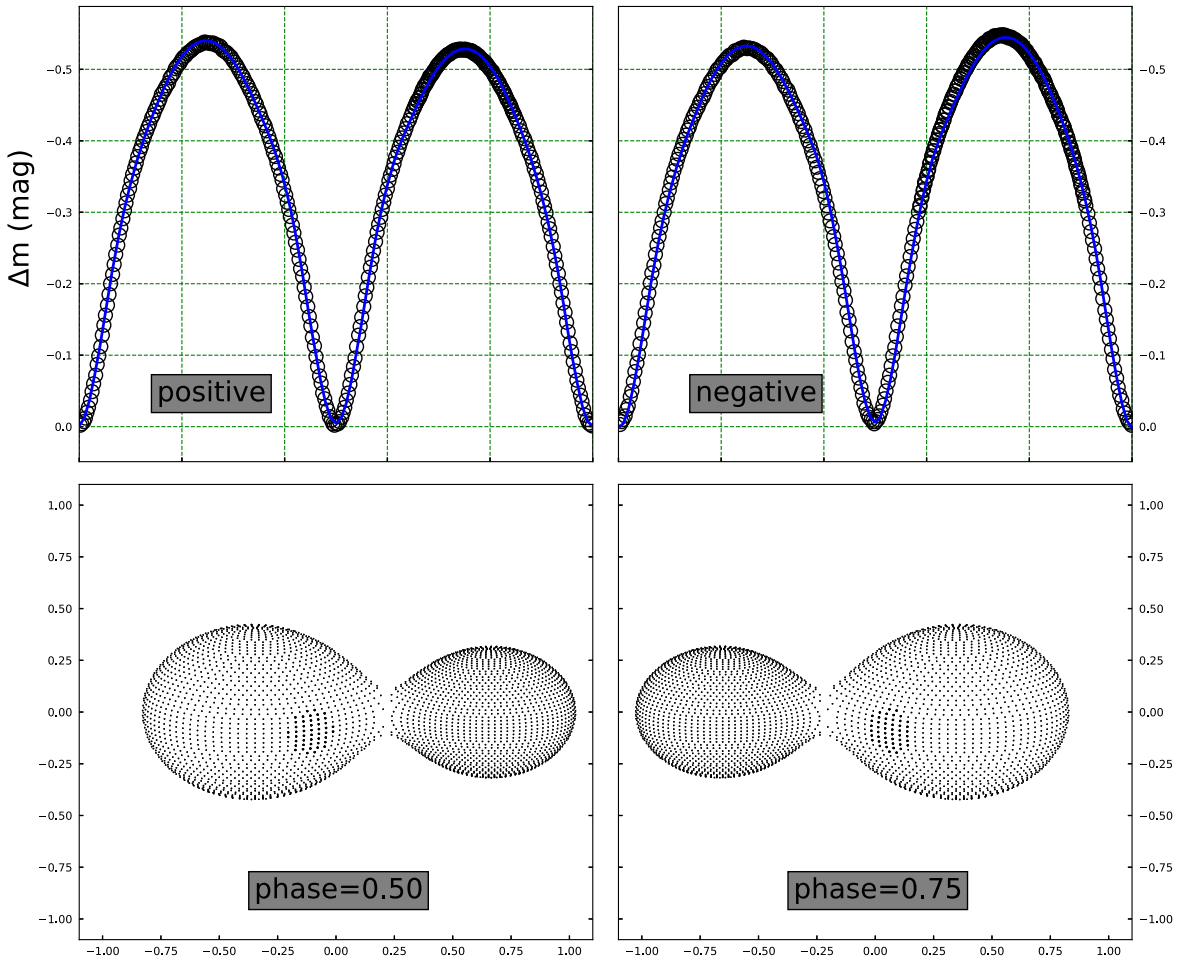

Figure 9. The theoretical light curves and the configurations for two typical O'Connell effect.

equation (Singh & Chaubey 1986),

$$\frac{\dot{P}}{P} = 3\dot{M}_2\left(\frac{1}{M_1} - \frac{1}{M_2}\right). \quad (4)$$

the mass transfer rate was determined to be $dM_2/dt = -8.67 \times 10^{-8}\,M_\odot\,\mathrm{yr}^{-1}$. Thus, the long-term increase of the orbital period is possibly due to the mass transfer from the less massive component to the more massive one. The cyclic oscillations ($A_3 = 0.00575$ days, $T_3 = 27.8$ yr) were typically explained by the light-travel time effect via a third body (Liao & Qian 2010; Qian et al. 2012, 2015). With the same method used by (Zhu et al. 2013a, 2013b). If the orbital inclination i' is 90°, the mass of the third body should be $m_3 = 0.201\,M_\odot$ with the maximal orbital radius of $a_3 = 11.55$ au.

Considering the cool spot on the surface of the primary component, Applegate (1992) suggested the oscillation could be due to magnetic activities. The quadrupole moment variations of the component stars were calculated by using these equations (Applegate 1992; Lanza & Rodonò 2002):

$$\frac{\Delta P}{P} = \frac{2\pi A_3}{T_3} = -9\frac{\Delta Q}{Ma^2}. \quad (5)$$

Here Q is the quadrupole moment, M for the mass of the active star and a for the semimajor axis of the orbit. For active components, $\Delta Q_1 = 5.93 \times 10^{49}\,\mathrm{g\,cm}^{-2}$ and $\Delta Q_2 = 3.03 \times 10^{49}\,\mathrm{g\,cm}^{-2}$ were determined, and similar to some active contact binary J082700 (Li et al. 2021), V694 Peg (Xu & Zhu 2014), OO Leo (Meng et al. 2024). Thus, the magnetic activity cycles of either of the components is one possible explanation for the periodic variation. We also explored the relations between the successive O'Connell effect from TESS data and $O - C$ trend, there is no correlation for them, consistent with these investigations on some binaries (Koju & Beaky 2015; Pi et al. 2019).

Table 5
Photometric Solutions of EF Boo

	Parameters	Elements	Errors	Parameters	Elements	Errors
	Mode	3	Assumed	Ω_{in}	2.93305	⋯
	T_1	6320 K	Assumed	Ω_{out}	2.61852	⋯
	LD	−3	Assumed	x_{1bol},y_{1bol}	0.541,0.638	Assumed
	q (M_2/M_1)	0.53	Assumed	x_{2bol},y_{2bol}	0.172,0.163	Assumed
	i	72.130	±0.048	$L_1/(L_1+L_2)$ (B)	0.6355	±0.0070
	T_2	6329 K	±3 K	$L_1/(L_1+L_2)$ (V)	0.6361	±0.0043
2020 LCs	$\Omega_1=\Omega_2$	2.86168	±0.00155	$L_1/(L_1+L_2)$ (R_c)	0.6363	±0.0034
	f	22.69%	±0.49%	$L_1/(L_1+L_2)$ (I_c)	0.6365	±0.0026
	$\Sigma\omega(O-C)^2$	0.0000041	⋯	⋯	⋯	⋯
	i	74.667	±0.048	ϕ_{spot}	90.°0	⋯
	T_2	6354 K	±4 K	λ_{spot}	50.°4	⋯
Positive LC	$\Omega_1=\Omega_2$	2.86340	±0.00133	R_{spot}	14.°3	⋯
	f	22.15%	±0.42%	τ_{spot}	0.92	⋯
	$\Sigma\omega(O-C)^2$	0.0000040	⋯	$L_1/(L_1+L_2)$ (TESS)	0.6323	±0.0007
	i	75.017	±0.085	ϕ_{spot}	90.°0	⋯
	T_2	6330 K	±8 K	λ_{spot}	302.7	⋯
Negative LC	$\Omega_1=\Omega_2$	2.86403	± 0.00233	R_{spot}	14.°3	⋯
	f	21.95%	± 0.74%	τ_{spot}	0.92	⋯
	$\Sigma\omega(O-C)^2$	0.0000170	⋯	$L_1/(L_1+L_2)$ (TESS)	0.6361	±0.0014

To understand the evolution and magnetic activity of contact binary EF Boo, the photometric monitoring is necessary to confirm their behaviors in light curves and orbital period in the future.

Acknowledgments

These photometric observations of EF Boo were obtained with ground-based telescopes and the TESS mission. We acknowledge the support of the staff of the 85 cm, 60 cm telescopes at the Xinglong observational station of the National Astronomical Observatories, Chinese Academy of Sciences, and TESS team works funding by the NASA Science Mission directorate. This work is sponsored by the Natural Science Foundation of Xinjiang Uygur Autonomous Region (No. 2022D01A164), by the National Natural Science Foundation of China (Nos. U1831109 and 12103030).

ORCID iDs

Jing-Jing Wang https://orcid.org/0000-0002-9947-9263
Bin Zhang https://orcid.org/0000-0001-7832-2972

References

Applegate, J. H. 1992, ApJ, 385, 621
Bakis, V., Erdem, A., Budding, E., & Demircan, O. 2003, IBVS, 5381, 1
Brt, L., Zejda, M., & Svoboda, P. 2007, OEJV, 74, 1
Banfi, M., Aceti, P., Arena, C., Bianciardi, G., et al. 2012, IBVS, 6033, 1
Bahar, E., Yorukoglu, O., Esmer, E. M., et al. 2017, IBVS, 6209, 1
Drozdz, M., & Ogloza, W. 2005, IBVS, 5623, 1
Dogru, S. S., Dogru, D., Erdem, A., Cicek, C., & Demircan, O. 2006, IBVS, 5707, 1
Dvorak, S. W. 2006, IBVS, 5677, 1
Diethelm, R. 2009, IBVS, 5894, 1
Diethelm, R. 2010, IBVS, 5920, 1
Diethelm, R. 2010, IBVS, 5945, 1
Diethelm, R. 2012, IBVS, 6029, 1
Eastman, J., Siverd, R., & Gaudi, B. S. 2010, PASP, 122, 935
Gothard, N. W., Van Hamme, W., & Samec, R. G. 2000, AAS Meeting Abstracts, 197, 48.03
Guilbault, P. R., Lloyd, C., & Paschke, A. 2001, IBVS, 5090, 1
Gazeas, K. D., Baran, A., Niarchos, P., et al. 2005, AcA, 55, 123
Hoeg, E., Bssgen, G., Bastian, U., et al. 1997, A&A, 323, 57
Hubscher, J., Braune, W., & Lehmann, P.B. 2013, IBVS, 6048, 1
Hubscher, J., Paschke, A., & Walter, F. 2005, IBVS, 5657, 1
Hubscher, J., Paschke, A., & Walter, F. 2006, IBVS, 5731, 1
Hubscher, J., Steinbach, H.M., & Walter, F. 2009, IBVS, 5874, 1
Hoňková, K., Juryšek, J., Lehký, M., et al. 2013, OEJV, 160, 1
Honkova, K., Jurysek, J., Lehky, M., et al. 2015, OEJV, 168, 1
Hubscher, J., & Lehmann, P. B. 2015, IBVS, 6149, 1
Hubscher, J. 2016, IBVS, 6157, 1
Hubscher, J. 2017, IBVS, 6196, 1
Hwang, H.-C., & Zakamska, N. L. 2020, MNRAS, 493, 2271
Heinze, A. 2023, AAS Meeting Abstracts, 241, 347.06
Irwin, J. B. 1952, ApJ, 116, 211
Krajci, T. 2005, IBVS, 5592, 1
Koju, V., & Beaky, M. M. 2015, IBVS, 6127, 1
Kouzuma, S. 2019, PASJ, 71, 21
Knote, M. F., Caballero-Nieves, S. M., Gokhale, V., Johnston, K. B., & Perlman, E. S. 2022, ApJS, 262, 10
Lanza, A. F., & Rodonò, M. 2002, AN, 323, 424
Li, K., Xia, Q-Q., Kim, C-H., et al. 2021, ApJ, 922, 122
Liao, W. P., & Qian, S. B. 2010, MNRAS, 405, 1930
Liu, Q.-Y., & Yang, Y.-L. 2003, CJAA, 3, 142
Lucy, L. B. 1967, ZAp, 65, 89
Meng, Z-B., Wu, P-R., Yu, Y-X., Hu, K., & Xiang, F-Y. 2024, ApJ, 971, 113
Mergentaler, J. 1950, Urani, 21, 58
Milone, E. E. 1968, AJ, 73, 708
Mullan, D. J. 1975, ApJ, 198, 563
Nelson, R. H. 2006, IBVS, 5672, 1

O'Connell, D. J. K. 1951, PRCO, 2, 85
Ozdemir, S., Demircan, O., Ciek, C., & Erdem, A. 2004, AN, 325, 332
Ozdemir, S., Demircan, O., Erdem, A., et al. 2001, IBVS, 5033, 1
Ozavci, I., Bahar, E., Izci, D. D., et al. 2019, OEJV, 203, 1
Perryman, M. A. C., Lindegren, L., Kovalevsky, J., et al. 1997, A&A, 323, L49
Pribulla, T., Vaňko, M., Chochol, D., Hambálek, L', & Parimucha, Š. 2011, AN, 332, 607
Papageorgiou, A., Kleftogiannis, G., & Christopoulou, P.-E. 2014, CoSka, 43, 470
Pagel, L. 2018, IBVS, 6244, 1
Pi, Q.-f., Zhang, L.-y., Bi, S.-l., et al. 2019, ApJ, 877, 75
Park, J.-H., Han, K.-Y., Jeong, T.-S., et al. 2024, OEJV, 250, 1
Qian, S. B., Han, Z. T., Fernndez Lajs, E., et al. 2015, ApJS, 221, 17
Qian, S. B., Liu, L., Zhu, L. Y., et al. 2012, MNRAS, 422, 24
Roberts, A. W. 1906, MNRAS, 66, 123
Ruciński, S. M. 1969, AcA, 19, 245
Rucinski, S. M., Lu, W., Mochnacki, S. W., Ogliza, W., & Stachowski, G. 2001, AJ, 122, 1974
Singh, M., & Chaubey, U. S. 1986, Ap&SS, 124, 389
Samec, R. G., Tuttle, J. P., Brougher, J. A., Moore, J. E., & Faulkner, D. R. 1999, IBVS, 4811, 1
Safar, J., & Zejda, M. 2002, IBVS, 5263, 1
Selam, S. O. 2004, A&A, 416, 1097
Sterken, C. 2005, in ASP Conf. Ser. 335, The Light-Time Effect in Astrophysics: Causes and Cures of the O-C Diagram, ed. C. Sterken (San Francisco, CA: ASP), 3
Samolyk, G. 2010, JAVSO, 38, 85
Stassun, K. G., Oelkers, R. J., Paegert, M., et al. 2019, AJ, 158, 138
Shi, X. D., Qian, S. B., Li, L. J., & Liu, N. P. 2021, AJ, 161, 46
Wilson, R. E., & Devinney, E. J. 1971, ApJ, 166, 605
Wilson, R. E. 1990, ApJ, 356, 613
Wilsey, N. J., & Beaky, M. M. 2009, SASS, 28, 107
Wilson, R. E., & Van Hamme, W. 2014, ApJ, 780, 151
Wilson, R. E. 2020, Galax, 8, 57
Xu, H.-S., & Zhu, L.-Y. 2024, ApJ, 975, 231
Yu, Y.-X., Zhang, X.-D., Hu, K., & Xiang, F.-Y. 2017, NewA, 55, 13
Yılmaz, M., Şenavcı, H. V., Bahar, E., et al. 2023, NewA, 101, 102022
Zejda, M. 2004, IBVS, 5583, 1
Zhu, L. Y., Qian, S. B., Liu, N. P., Liu, L., & Jiang, L. Q. 2013a, AJ, 145, 39
Zhu, L.-Y., Qian, S.-B., Zhou, X., et al. 2013b, AJ, 146, 28
Zhang, L.-Y., Pi, Q.-F., & Yang, Y.-G. 2014, MNRAS, 442, 2620
Zhou, A. Y., Jiang, X. J., Zhang, Y. P., & Wei, J. Y. 2009, RAA, 9, 349